Detecting quadratically coupled ultralight dark matter with stimulated annihilation

Yuanlin Gong,[1,*] Xin Liu,[1,†] Lei Wu,[1,‡] Qiaoli Yang,[2,§] and Bin Zhu[3,‖]

[1]*Department of Physics and Institute of Theoretical Physics, Nanjing Normal University, Nanjing 210023, China*

[2]*Siyuan Laboratory and Department of Physics, Jinan University, Guangzhou 510632, China*

[3]*Department of Physics, Yantai University, Yantai 264005, China*

(Received 2 November 2023; accepted 12 February 2024; published 14 March 2024)

Ultralight dark matter (ULDM) is one of the most promising DM candidates. Because of the Bose enhancement, we find the annihilation rate of ULDM in the presence of background photon radiation can be greatly enhanced and produce a distinctive reflected electromagnetic wave with an angular frequency equal to the ULDM mass. We propose to utilize such stimulated annihilation to probe the ULDM with the electromagnetic quadratic coupling by emitting a radio beam into space. With a power of a 50 MW emitter, we forecast the sensitivity of quadratic coupling in different local halo models for low-frequency radio telescopes, such as LOFAR, UTR-2, and ngLOBO.

DOI: 10.1103/PhysRevD.109.055026

I. INTRODUCTION

Dark matter, the invisible substance accounting for more than 80% of the matter in the Universe, continues to be a compelling mystery in modern physics [1]. The extensively studied canonical cold dark matter models, represented by weakly interacting massive particles (WIMPs), are attractive, providing the correct relic abundance and simultaneously solving other modern puzzles, such as the hierarchy problem [2]. However, the recent null experiment results put increasingly stringent constraints on various WIMP models [3].

The ultralight dark matter (ULDM) that features a spin-0 particle with a mass ranging from 10^{-24} to 1 eV is a competitive alternative, which could be produced through the misalignment mechanism or its variants in the early Universe [4–8]. The wavelike nature of these particles can not only preserve the merits of cold dark matter, but also may provide a solution to the small-scale structure problem [9–11]. Moreover, recent studies on the Galactic scale, such as gravitationally lensed images, indicates the increasing success of the wavelike DM versus the particlelike DM [12]. Additionally, the ULDM also possibly addresses the strong *CP* problem [13–16], aforementioned hierarchy problem [17], and dark energy [18–20].

The distribution of the ULDM near Earth is crucial for its detection in laboratory experiments. Aside from the DM halo of the Milky Way halo [21–23], the caustic ring model describing the full phase-space distribution of the Milky Way is also well motivated and established [24–26]. It results in the occurrence of flows with varying density and dispersion near Earth. On the other hand, the formation of a local ULDM dark halo [27–29] bound to other gravitational sources, such as the Sun and Earth, provides an alternative profile possibility. The Sun halo and Earth halo result in much higher dark matter densities around the Earth's vicinity compared to the Milky Way halo over a wide mass range, which could significantly affect the sensitivity of ULDM detection.

Note that the approaches to detecting the ULDM strongly depend on its interactions with the Standard Model (SM) particles. Generically, the linear couplings of the ULDM with the SM particles are dominant, however, which have been tightly constrained by atom clocks [30–34], atomic spectroscopy [35–39], laser interferometry [40,41], gravitational-wave detectors [42–44], astrophysical probes [45–50], and others [51–57]. Additionally, the enhanced emission of the axion clusters or axionlike particles may provide a complementary bound [58–60]. On the other hand, the quadratic interactions of the ULDM dominating over the linear ones in recent years have drawn particular interest, such as in theories with $\mathbb{Z}_N$ symmetry [61,62] and the relaxion mechanism [63]. Despite the above experimental

*yuanlingong@nnu.edu.cn
†liuxin@njnu.edu.cn
‡leiwu@njnu.edu.cn
§qiaoliyang@jnu.edu.cn
‖zhubin@mail.nankai.edu.cn

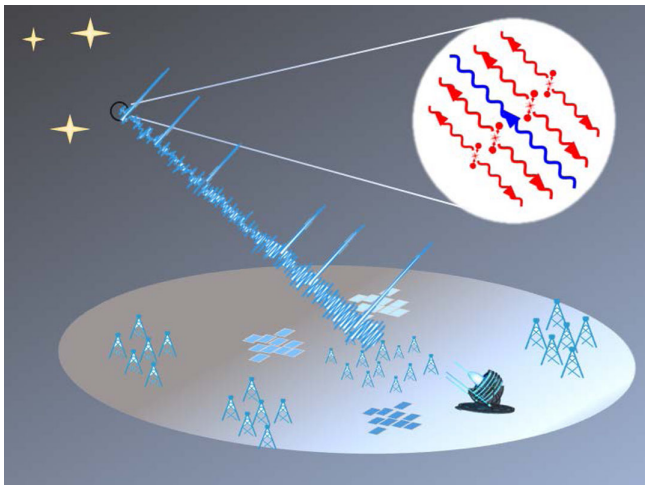

FIG. 1. Conceptual design of our proposed experiment. A powerful radio beam (blue wavy line) is sent to space to stimulate the annihilation of the ULDM (red bullet). The reflected radio (red wavy line) will be detected by the array telescope.

bounds, the parameter space of the quadratic interactions remains largely unexplored.

In this article, we propose to probe the quadratic interaction of ULDM by detecting the reflected electromagnetic wave signal produced from the stimulated annihilation (as shown in Fig. 1). In contrast to the spontaneous process, the flux of photons from the stimulated annihilation can be greatly enhanced by the presence of ambient photons, due to Bose enhancement. Since the power for signal photons highly depends on the local DM density, we consider four different local DM halos in our analysis: the isothermal halo, the caustic ring model, the Sun halo, and the Earth halo. By using a radio emitter with a power of 50 MW and low-frequency radio telescopes, we present the new projected limit of the quadratic coupling of ULDM in the mass range of $2.07 \times 10^{-8} \sim 1 \times 10^{-6}$ eV for all of the halos.

II. STIMULATED ANNIHILATION

The quadratic interaction of the ULDM field ϕ with the electromagnetic fields A_μ is given by

$$\mathcal{L} = \frac{d_e^{(2)}}{4} \frac{2\pi}{M_{\rm Pl}^2} \phi^2 F_{\mu\nu} F^{\mu\nu}, \tag{1}$$

where the field strength $F^{\mu\nu} = \partial^\mu A^\nu - \partial^\nu A^\mu$, $d_e^{(2)}$ is the quadratic coupling constant, and $M_{\rm Pl} = 1.22 \times 10^{19}$ GeV is the Planck mass (for the pseudoscalar case, see [64]). For simplicity, we assume $g' = \frac{2\pi}{M_{\rm Pl}^2} d_e^{(2)}$ in our calculations. Since the DM is nonrelativistic in the halo, the angular frequency of the ULDM is approximate to its mass, $\omega_\phi = m_\phi$. With Eq. (1), we can have the cross section of the spontaneous annihilation process $\phi\phi \to \gamma\gamma$,

$$\sigma_0 = \frac{1}{32\pi} \frac{1}{\beta} g'^2 m_\phi^2, \tag{2}$$

where the factor β is the velocity of ULDM. Because of the tiny coupling and the small mass of the ULDM, the spontaneous annihilation rate is highly suppressed. We note that a certain incoming photon can stimulate the annihilation of the ULDM and thus produce an observable electromagnetic signal. There are two methodologies to describe the stimulated emission: (1) One involves the Boltzmann equation where the spontaneous annihilation amplitude of ULDM is enhanced by the Bose enhancement from the indistinguishability of identical bosons [59,60,65]. (2) The other one resorts to the modified electrodynamics, where the question becomes a radiation problem. The effective current density is provided by the interaction in Eq. (1). The ϕ manifests itself as a classical coherent field and the stimulated enhancement is described through the resonance [64,66]. We continue our proposal in method 1, while giving the derivation in method 2 in the Supplemental Material [67].

To obtain the production rate of the photons from stimulated annihilation, we first consider the number of states in the phase space of the spontaneous annihilation process $\phi\phi \to \gamma\gamma$. In the vacuum, there are f_ϕ ULDM with the certain momentum and zero photons in the phase space of the initial states. After annihilation, the final state will contain $(f_\phi - 1)$ ULDM and two photons with two directions of momentum that are antiparallel to each other in the center-of-mass frame of the two ULDM, i.e., $|\mathrm{i}\rangle_0 = |f_\phi, f_\phi; 0, 0\rangle$, $|\mathrm{f}\rangle_0 = |f_\phi - 1, f_\phi - 1; 1, 1\rangle$. However, due to the Bose enhancement of identical photons, if the annihilation occurs in the background of f_γ photons, this process will be stimulated and leads to

$$\begin{aligned} |\mathrm{i}\rangle &= |f_\phi, f_\phi; f_\gamma, f_\gamma\rangle, \\ |\mathrm{f}\rangle &= |f_\phi - 1, f_\phi - 1; f_\gamma + 1, f_\gamma + 1\rangle. \end{aligned} \tag{3}$$

Then, we can have the scattering amplitude of the stimulated annihilation,

$$\mathcal{M}_{\mathrm{i}\to\mathrm{f}} = \mathcal{M}_0^\dagger f_\phi (f_\gamma + 1), \tag{4}$$

where $\mathcal{M}_0$ is the spontaneous annihilation amplitude. The inverse process of two photons annihilating to two ULDM in the vicinity of f_γ ambient photons corresponds to the following matrix element:

$$\mathcal{M}_{\mathrm{f}\to\mathrm{i}} = \mathcal{M}_0 (f_\phi + 1) f_\gamma. \tag{5}$$

In the presence of ambient photons, the effective annihilation amplitude for the stimulated annihilation of the ULDM is determined by the difference between the amplitude of the annihilation and production processes of the photons as follows:

$$|\mathcal{M}_{\mathrm{i}\to\mathrm{f}}|^2 - |\mathcal{M}_{\mathrm{f}\to\mathrm{i}}|^2 = |\mathcal{M}_0|^2[f_\phi^2(f_\gamma+1)^2 - (f_\phi+1)^2 f_\gamma^2],$$
$$= |\mathcal{M}_0|^2[f_\phi^2 + 2f_\gamma f_\phi^2 - 2f_\phi f_\gamma^2 - f_\gamma^2],$$
$$\approx |\mathcal{M}_0|^2 f_\phi^2(1+2f_\gamma). \tag{6}$$

The four terms in the second line are interpreted as the contributions from spontaneous annihilation, stimulated annihilation, inverse stimulated annihilation, and inverse spontaneous annihilation. It is then clear that the factor $2f_\gamma$ is the enhancement for stimulated annihilation compared to spontaneous annihilation. We have used the approximation $f_\phi \gg f_\gamma$ in the last line.

From the Boltzmann equation, we can obtain the annihilation rate of the ULDM from the stimulated annihilation process $\phi(p_1)\phi(p_2) \to \gamma(k_1)\gamma(k_2)$,

$$\dot{n}_\phi = -\int d\Pi_\phi d\Pi_\phi d\Pi_\gamma d\Pi_\gamma (2\pi)^4\delta^4(p_1+p_2-k_1-k_2)$$
$$\times\frac{1}{4}\cdot[|\mathcal{M}_{\mathrm{i}\to\mathrm{f}}|^2 - |\mathcal{M}_{\mathrm{f}\to\mathrm{i}}|^2]$$
$$= -4\beta n_\phi^2\sigma_0(1+2f_\gamma), \tag{7}$$

where $d\Pi_i = g_i dp^3/((2\pi)^3\cdot 2E_i)$ is the usual phase-space volume. The factor of $1/4$ in the first line is the symmetry factor for identical particles in the initial and final states. n_i is the number density of the ULDM or the photon, which is related to phase-space distribution by $n_i = \int \frac{g_i}{(2\pi)^3} f_i(\mathbf{p}) d^3p_i$. The production rate of the photons is the negative of the annihilation rate of the ULDM. This is greatly enhanced by the factor $2f_\gamma$, which arises from the stimulation of the ambient photons as $\omega_\gamma = m_\phi$. Moreover, the production rate of the photons depends on the ULDM density as ρ_{DM}^2, rather than ρ_{DM}.

A straightforward consideration inspired by the Bose enhancement and substantial occupation number of the ULDM is the more intriguing process of n ULDM scatter into two photons arising from the effective interactions described by the Lagrangian $\mathcal{L} = \frac{1}{4}\frac{d_e^{(n)}}{M_{\mathrm{Pl}}^n}\phi^n F_{\mu\nu}F^{\mu\nu}$, since the annihilation rate of the ULDM will be dependent on n_ϕ^n, being potentially huge at first glance. A closer derivation results in $\dot{n}_\phi$ being proportional to the factor $F = (\frac{\rho_\phi}{2M_{\mathrm{Pl}}^2 m_\phi^2})^n \frac{n^4}{n!}$. We find that this factor decreases in power with n for the $m_\phi > 1.07\times10^{-31}$ eV for all the halo models we considered here, despite the much higher density ρ_ϕ in the Earth and Sun halos at some mass ranges. For the lower mass ranges, the ULDM cannot be all dark matter and are constrained by the Galaxy Structure formation. Thus, as claimed before [61–63], in the scenarios where the linear order $n=1$ is absent, the dominant contribution naturally emanates from the quadratic $n=2$ order, which is the focus of this work.

III. SIGNAL POWER

The signal power received by the telescope can be obtained by integrating Eq. (7) over time, the solid angle along the direction of the outgoing emission beam, the frequency, and the area

$$P = -\int dA d\nu d\Omega \int_0^{t_{\mathrm{off}}} dt \dot{n}_\phi,$$
$$= \frac{1}{8}\frac{g'^2}{m_\phi^2}\frac{P_0}{\Delta\nu_\phi}\int_0^{t_{\mathrm{off}}}\rho_\phi^2 dt, \tag{8}$$

where the duration time of emission is denoted as t_{off}. We ignored the interaction between the photon and the electron in the environment and factorized out the power of the source as

$$P_0 = \int dA d\nu d\Omega n_\gamma. \tag{9}$$

Here we assume that f_γ is a Gaussian-like function with an expected value ω_γ and is related to $n_\gamma = \frac{2}{(2\pi)^3}4\pi\omega_\gamma^2\Delta\omega_\gamma f_\gamma$ by averaging it over the bandwidth $\Delta\omega_\gamma = \Delta\omega_\phi \equiv 2\pi\Delta\nu_\phi$, with the ULDM bandwidth $\Delta\nu_\phi = 2\nu_\phi\sigma_v$ depending on the velocity dispersion σ_v of the ULDM [59,60,65]. Note that P_0 is only determined by the properties of the emitter. In addition, it can be seen that the signal power P in Eq. (8) is sensitive to the local density of the ULDM halo, which is commonly assumed to be the isothermal DM halo. However, the distribution of ULDM in the Milky Way may differ from the predictions of the isothermal DM halo. The simulation for the formation of the Galactic halo suggests the enhancement (or suppression) of the local DM density due to the formation of "clumps" or streams [68]. Owing to the self-interactions or topological properties of the ULDM, the possibility of the formation of condensates [69], clusters [70], boson stars [27–29,71], or domain walls [31,72] has been discussed. Their impact on the detection of ULDM was considered in [32] for deep space atomic clocks, in [37,38] for atomic spectroscopy, in [44] for gravitational-wave detectors, and in [73] with neutrino oscillations. In our phenomenological study, we consider four different halo models.

(i) Isothermal halo model: This standard density model of the Milky Way from N-body simulations predicts a local energy density of $\rho_I \approx 0.3$ GeV/cm^3 with velocity dispersion of $\sigma_I = 270/\sqrt{3}$ km/s [21–23].
(ii) Caustic ring model: Motivated by the description of the full phase-space distribution of the Milky Way halo, the caustic ring model predicts the configuration of the caustics and flows [24]. The properties of the flows are constrained by the observations of the Infrared Astronomical Satellite and Gaia maps [26]. The resulting local dark matter velocity distribution is dominated by the big flow with velocity dispersion less

than $\sigma_c = 70$ m/s [25] and density as high as $\rho_c = 10\ \mathrm{GeV/cm^3}$ [26].

(iii) Sun halo model: As an extension of the boson star, it has been recently discussed in [27–29,32]. This was initially motivated by the suggestion from the large-scale numerical simulations of Galaxy formation for fuzzy dark matter ($m_\phi \sim 10^{-22}$ eV) without [74,75] and with [76] the presence of baryons that halolike configurations can form in the central cores of galaxies. In the presence of quartic self-interactions and subsequent gravitational focusing, an external gravitational source, such as the Sun, in the background of virialized DM, can effectively capture the ULDM to form an overdensity local halo. For the mass range of our interest ($m > 10^{-9}$ eV, see below), its density $\rho_{\rm sh}$ around Earth is much lower than that of the isothermal halo and decreases exponentially with the increase in the ULDM mass. The velocity dispersion is $1/(m_\phi R_{\rm sh})$, where $R_{\rm sh}$ is the radius of the Sun halo.

(iv) Earth halo model: Similar to the Sun halo model, it is also discussed in [27–29,32]. Reference [27] showed that the maximally allowed value of the energy density $\rho_{\rm eh}$ of the Earth halo is given by

$$\rho_{\rm eh}(r) \propto \begin{cases} \exp\left(-2r/R_{\rm eh}\right) & \text{for } R_{\rm eh} > R_{\rm E}, \\ \exp\left(-r^2/R_{\rm eh}^2\right) & \text{for } R_{\rm eh} \le R_{\rm E}. \end{cases} \tag{10}$$

Here $R_{\rm eh}$ is the radius of the Earth halo, which is a function of the ULDM mass [27]. $R_{\rm E}$ is the radius of Earth. As a comparison with the isothermal DM halo, the Earth halo has a much higher density. On the other hand, with the increase in the ULDM mass, the Earth halo density decreases exponentially. For the estimation below, we take Fig. 2 in the Supplemental Material of [27], which provides a detailed description of the maximally allowed value of energy density $\rho_{\rm eh}$.

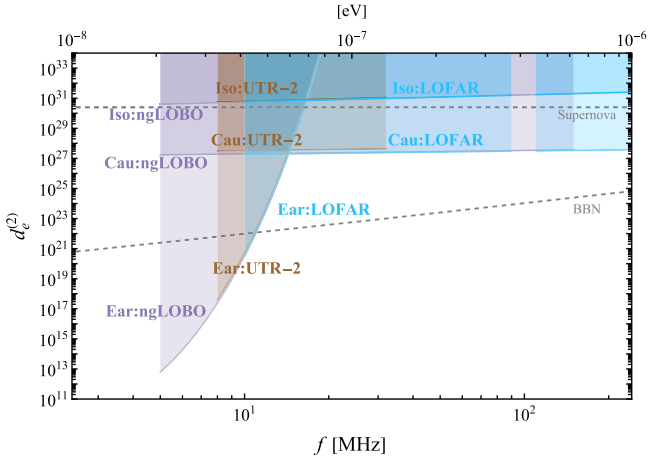

FIG. 2. The expected bounds on the plane of the dimensionless coupling $d_e^{(2)}$ versus the ULDM mass m_ϕ for the isothermal halo, caustic ring model, and the Earth halo. The array telescopes LOFAR, UTR-2, and ngLOBO are considered here. The gray dashed lines are the limits from the BBN and supernova [36].

IV. RESULTS AND DISCUSSIONS

In this work, our frequency range of interest is about 5–240 MHz. For lower frequencies, the impact of the ionosphere will become significant, while for higher frequencies, the signal will be suppressed by the mass of the ULDM as is seen in Eq. (8). To detect such low-frequency radio signals, we use the LOFAR [77], UTR-2 [78], and ngLOBO [79] to estimate the sensitivity. LOFAR, as one of the new-generation radio telescopes, is capable of detecting radio signals in the frequency ranges of 10–90 and 110–240 MHz with an unparalleled sensitivity owing to the novel phased-array design, dense core array, and long interferometric baselines [77,80]. Different from the traditional dish telescope, a number of dipole antenna elements are well arranged to compose a circular array with a diameter of 70–80 m, which enables it to observe in several modes and to detect the transient pulse signal with its high time and frequency resolution. The minimal frequency resolution of LOFAR is about 700 Hz [77]. As for the UTR-2, a T-shaped antenna array can achieve a lower operating frequency range 8–32 MHz with a frequency resolution down to 4 kHz [78]. The low band of the ngLOBO is to cover the frequency range 5–150 MHz [79], the resolution of which can reach 1 kHz at least [81,82]. The relevant parameters of the three telescopes are given in Table I.

The noise power of a radio array telescope with a frequency bandwidth Δ during the observing time $t_{\rm off}$ reads [83]

$$P_{\rm n} = \frac{2kT_{\rm sys}}{\eta_{\rm s}}\sqrt{\frac{\Delta}{n_{\rm pol}t_{\rm off}}}, \tag{11}$$

where k is the Boltzmann constant and $n_{\rm pol} = 2, 1, 2$ is the number of polarizations for LOFAR [77], UTR-2 [78], and ngLOBO [81,82], respectively. For simplicity, we assume the detection efficiency $\eta_s = 1$ in our numerical calculations. The bandwidth is determined by $\Delta = \max(\Delta\nu_\phi, \Delta\nu_{\rm res})$, where $\Delta\nu_{\rm res}$ is the telescope frequency resolution. $T_{\rm sys}$ is the temperature of the array system.

TABLE I. The frequency range, maximum system temperature $T_{\rm sys,m}$, and frequency resolution $\Delta\nu_{\rm res}$ for LOFAR [77], UTR-2 [78], and ngLOBO [79]. The values of $T_{\rm sys,m}$ are evaluated at the frequencies $\nu = 10$, $\nu = 110$, $\nu = 8$, and $\nu = 5$ MHz.

Telescope	Frequency (MHz)	$T_{\rm sys,m}$ (K)	$\Delta\nu_{\rm res}$ (kHz)
LOFAR	10–90	3.5×10^5	0.7
LOFAR	110–240	766	0.7
UTR-2	8–32	6.1×10^5	4
ngLOBO	5–150	2.0×10^6	≤1

It is caused by several inevitable noises, such as the cosmic microwave background, the environment, the galaxy, and the instrument. Among them, galaxy noise is dominant [84]. Then, we approximate the system temperature as $T_{\rm sys} \approx 1.23 \times 10^8\ {\rm K}({\rm MHz}/\nu)^{2.55}$, where ν is the frequency of the noise photon [77,84].

Additionally, the transverse velocity $\vec{v}_\perp$ of the ULDM perpendicular to the outgoing radio beam will result in the displacement of the reflected radio signal from the location of the outgoing power source. Thus, the duration time $t_{\rm off}$ in Eq. (8) should be less than the effective time $t_{\rm eff} = C\frac{R}{\langle|\vec{v}_\perp|\rangle}$, where R is the radius of the array telescope. In the frequency range of our interest, $\langle|\vec{v}_\perp|\rangle$ is about 124 km/s for the isothermal halo [64], about 5 km/s for the caustic ring model [26], and about 1.2 km/s for the Earth halo [27]. For the Sun halo, the contribution for transverse velocity comes from velocity $v_{\rm s} = 1.1$ km/s of ULDM in the frame of the Sun and the relative velocity $v_{\rm r} \approx 29$ km/s between the Sun and Earth. Thus, we take $\langle|\vec{v}_\perp|\rangle = 30$ km/s. In reality, the geometry factor C depends on the specific configuration of the emitter relative to the collector in the experiment. Here we take $C = 0.3$ to estimate the sensitivity. Since the height of the ionosphere is approximately 48 km, the time required for a radio wave pointing to the telescope to travel from the ionosphere to the telescope is 160 μs, which is greater than the effective time for the isothermal halo and not much smaller than that of the caustic ring and the Sun halos. Meanwhile, we note that the density of the Earth halo will vanish before the radio reaches the ionosphere. Therefore, it is justifiable to disregard the interaction between photons and electrons in the environment.

For an emitter with power P_0, we can have the total energy consumption $E_0 = NP_0t_{\rm off}$, where $N = m_\phi/2\Delta\nu_\phi$ is the emission times. In the following calculations, we set $E_0 = 10$ MW yr, $P_0 = 50$ MW, and $R = 50$ m. By requiring $P > P_{\rm n}$, we can obtain the exclusion limit of the dimensionless coupling $d_e^{(2)}$,

$$d_e^{(2)} < D \cdot \left(\frac{50\ {\rm MW}}{P_0}\frac{T_{\rm sys}}{3.5\times10^5\ {\rm K}}\right)^{\frac{1}{2}} \cdot \left(\frac{\Delta}{n_{\rm plo}}\right)^{\frac{1}{4}} \tag{12}$$

with

$$D = \begin{cases} 7.43\times10^{28}\cdot\left(\frac{4219\ {\rm sec}}{t_{\rm off}}\right)^{\frac{1}{4}}\left(\frac{m_\phi^3}{{\rm GeV}^3}\frac{{\rm GeV}^7}{\rho_{\rm I}^2 t_{\rm eff}}\right)^{\frac{1}{2}}, & \text{Isothermal} \\ 9.24\times10^{27}\cdot\left(\frac{1\ {\rm sec}}{t_{\rm off}}\right)^{\frac{1}{4}}\left(\frac{m_\phi^3}{{\rm GeV}^3}\frac{{\rm GeV}^7}{\rho_{\rm c}^2 t_{\rm eff}}\right)^{\frac{1}{2}}, & \text{Caustic} \\ 1.80\times10^{28}\cdot\left(\frac{14.7\ {\rm sec}}{t_{\rm off}}\right)^{\frac{1}{4}}\left(\frac{m_\phi^3}{{\rm GeV}^3}\frac{{\rm GeV}^7}{\int_0^{t_{\rm eff}}\rho_{\rm sh}^2 dt}\right)^{\frac{1}{2}}, & \text{Sun} \\ 1.85\times10^{28}\cdot\left(\frac{16\ {\rm sec}}{t_{\rm off}}\right)^{\frac{1}{4}}\left(\frac{m_\phi^3}{{\rm GeV}^3}\frac{{\rm GeV}^7}{\int_0^{t_{\rm eff}}\rho_{\rm eh}^2 dt}\right)^{\frac{1}{2}}, & \text{Earth.} \end{cases} \tag{13}$$

For the isothermal halo, we can take $\Delta = \Delta\nu_\phi$. It is because the bandwidth of the ULDM is scaled as $15.09\ {\rm kHz}\cdot(m/0.03\ \mu{\rm eV})$, which is larger than the frequency resolution of the LOFAR, UTR-2, and ngLOBO. While for the caustic ring model, the Sun halo, and the Earth halo, since the frequency resolution $\Delta\nu_{\rm res}$ is larger than the bandwidth $\Delta\nu_\phi$ of ULDM in our mass range, we take $\Delta = 0.7$, 1, and 4 kHz in Eq. (12) for LOFAR, UTR-2, and ngLOBO, respectively.

The resulting expected exclusion limits are shown in Fig. 2. We can see that the bounds for the quadratic coupling $d_e^{(2)}$ strongly depend on the ULDM halo models. They are around $d_e^{(2)} < 10^{27}$ and 10^{30} in the caustic ring model and the isothermal halo, respectively. The bounds for the isothermal halo are weaker than the limits from the big bang nucleosynthesis (BBN) and supernova [36], while that for the isothermal halo are weaker than the limit from BBN, but stronger that the limit from supernova by 2–3 orders of magnitude. Since the density of the Sun halo is very low in our mass range, the corresponding constraint is much weaker than others and thus is not shown. On the other hand, the limit on $d_e^{(2)}$ in the Earth halo model can be 10^{13}–10^{34} in the range of $2.07\times10^{-8} < m_\phi < 8.27\times10^{-8}$ eV $(5 < f < 20$ MHz). The limits in this range can be at most 8 orders of magnitude stronger than that of the BBN and at most 17 orders of magnitude stronger than that of the supernova. All the limits shown weaken with the increasing mass. Since the ULDM bandwidth $\Delta\nu_\phi$ for the caustic ring model is larger than the telescope frequency resolution $\Delta\nu_{\rm res}$ in the higher mass range, we should take $\Delta = \Delta\nu_\phi$ in these mass range and the limits on the caustic ring model will be further suppressed. With the improved measurement of the Gaia maps [85], a more precise local DM distribution can be reached and reduce the uncertainty in the search for DM in the future. Additionally, we note that the sensitivity can be further enhanced by increasing the power of the emitter and enlarging the array telescope radius. In addition, a better frequency resolution of the telescope will improve the results in the same work frequency.

ACKNOWLEDGMENTS

Y. G. would like to thank Ariel Arza and Hyungjin Kim for useful discussions. This work is supported by the National Natural Science Foundation of China (NNSFC) under Grants No. 12275134, No. 12335005, No. 12275232, No. 12147228, and No. 12150010.

[1] G. Bertone, D. Hooper, and J. Silk, Phys. Rep. **405**, 279 (2005).
[2] G. Jungman, M. Kamionkowski, and K. Griest, Phys. Rep. **267**, 195 (1996).
[3] L. Roszkowski, E. M. Sessolo, and S. Trojanowski, Rep. Prog. Phys. **81**, 066201 (2018).
[4] J. Preskill, M. B. Wise, and F. Wilczek, Phys. Lett. B **120B**, 127 (1983).
[5] L. F. Abbott and P. Sikivie, Phys. Lett. B **120B**, 133 (1983).
[6] M. Dine and W. Fischler, Phys. Lett. **120B**, 137 (1983).
[7] N. Herring, D. Boyanovsky, and A. R. Zentner, Phys. Rev. D **101**, 083516 (2020).
[8] B. Batell and A. Ghalsasi, Phys. Rev. D **107**, L091701 (2023).
[9] W. Hu, R. Barkana, and A. Gruzinov, Phys. Rev. Lett. **85**, 1158 (2000).
[10] L. Hui, J. P. Ostriker, S. Tremaine, and E. Witten, Phys. Rev. D **95**, 043541 (2017).
[11] E. G. M. Ferreira, Astron. Astrophys. Rev. **29**, 7 (2021).
[12] A. Amruth *et al.*, Nat. Astron. **7**, 736 (2023).
[13] R. D. Peccei and H. R. Quinn, Phys. Rev. Lett. **38**, 1440 (1977).
[14] R. D. Peccei and H. R. Quinn, Phys. Rev. D **16**, 1791 (1977).
[15] S. Weinberg, Phys. Rev. Lett. **40**, 223 (1978).
[16] F. Wilczek, Phys. Rev. Lett. **40**, 279 (1978).
[17] P. W. Graham, D. E. Kaplan, and S. Rajendran, Phys. Rev. Lett. **115**, 221801 (2015).
[18] R. D. Peccei, J. Sola, and C. Wetterich, Phys. Lett. B **195**, 183 (1987).
[19] J. A. Frieman, C. T. Hill, A. Stebbins, and I. Waga, Phys. Rev. Lett. **75**, 2077 (1995).
[20] E. G. M. Ferreira, G. Franzmann, J. Khoury, and R. Brandenberger, J. Cosmol. Astropart. Phys. 08 (2019) 027.
[21] M. S. Turner, Phys. Rev. D **33**, 889 (1986).
[22] J. F. Navarro, C. S. Frenk, and S. D. M. White, Astrophys. J. **490**, 493 (1997).
[23] M. Pato and F. Iocco, Astrophys. J. Lett. **803**, L3 (2015).
[24] L. D. Duffy and P. Sikivie, Phys. Rev. D **78**, 063508 (2008).
[25] N. Banik and P. Sikivie, Phys. Rev. D **93**, 103509 (2016).
[26] S. S. Chakrabarty, Y. Han, A. H. Gonzalez, and P. Sikivie, Phys. Dark Universe **33**, 100838 (2021).
[27] A. Banerjee, D. Budker, J. Eby, H. Kim, and G. Perez, Commun. Phys. **3**, 1 (2020).
[28] A. Banerjee, D. Budker, J. Eby, V. V. Flambaum, H. Kim, O. Matsedonskyi, and G. Perez, J. High Energy Phys. 09 (2020) 004.
[29] D. Budker, J. Eby, M. Gorghetto, M. Jiang, and G. Perez, J. Cosmol. Astropart. Phys. 12 (**2023**) 021.
[30] A. Arvanitaki, J. Huang, and K. Van Tilburg, Phys. Rev. D **91**, 015015 (2015).
[31] A. Derevianko and M. Pospelov, Nat. Phys. **10**, 933 (2014).
[32] Y.-D. Tsai, J. Eby, and M. S. Safronova, Nat. Astron. **7**, 113 (2023).
[33] S. Aharony, N. Akerman, R. Ozeri, G. Perez, I. Savoray, and R. Shaniv, Phys. Rev. D **103**, 075017 (2021).
[34] A. A. Geraci, C. Bradley, D. Gao, J. Weinstein, and A. Derevianko, Phys. Rev. Lett. **123**, 031304 (2019).
[35] K. Van Tilburg, N. Leefer, L. Bougas, and D. Budker, Phys. Rev. Lett. **115**, 011802 (2015).
[36] Y. V. Stadnik and V. V. Flambaum, Phys. Rev. Lett. **115**, 201301 (2015).
[37] D. Antypas, O. Tretiak, A. Garcon, R. Ozeri, G. Perez, and D. Budker, Phys. Rev. Lett. **123**, 141102 (2019).
[38] O. Tretiak, X. Zhang, N. L. Figueroa, D. Antypas, A. Brogna, A. Banerjee, G. Perez, and D. Budker, Phys. Rev. Lett. **129**, 031301 (2022).
[39] Y. V. Stadnik, Phys. Rev. Lett. **131**, 011001 (2023).
[40] Y. V. Stadnik and V. V. Flambaum, Phys. Rev. Lett. **114**, 161301 (2015).
[41] A. A. Geraci and A. Derevianko, Phys. Rev. Lett. **117**, 261301 (2016).
[42] A. Arvanitaki, P. W. Graham, J. M. Hogan, S. Rajendran, and K. Van Tilburg, Phys. Rev. D **97**, 075020 (2018).
[43] H. Grote and Y. V. Stadnik, Phys. Rev. Res. **1**, 033187 (2019).
[44] S. M. Vermeulen *et al.*, Nature (London) **600**, 424 (2021).
[45] K. A. Olive and M. Pospelov, Phys. Rev. D **77**, 043524 (2008).
[46] A. Berlin, Phys. Rev. Lett. **117**, 231801 (2016).
[47] A. Khmelnitsky and V. Rubakov, J. Cosmol. Astropart. Phys. 02 (2014) 019.
[48] D. Blas, D. L. Nacir, and S. Sibiryakov, Phys. Rev. Lett. **118**, 261102 (2017).
[49] P. Athron *et al.*, J. High Energy Phys. 05 (2021) 159.
[50] G.-W. Yuan, Z.-Q. Shen, Y.-L. S. Tsai, Q. Yuan, and Y.-Z. Fan, Phys. Rev. D **106**, 103024 (2022).
[51] E. Savalle, A. Hees, F. Frank, E. Cantin, P.-E. Pottie, B. M. Roberts, L. Cros, B. T. Mcallister, and P. Wolf, Phys. Rev. Lett. **126**, 051301 (2021).
[52] R. Oswald *et al.*, Phys. Rev. Lett. **129**, 031302 (2022).
[53] J. Ren, D. Wang, L. Wu, J. M. Yang, and M. Zhang, J. High Energy Phys. 11 (2021) 138.
[54] Y. Gu, L. Wu, and B. Zhu, Phys. Rev. D **105**, 095008 (2022).
[55] L. Su, L. Wu, and B. Zhu, Phys. Rev. D **105**, 055021 (2022).
[56] D. Wang, L. Wu, J. M. Yang, and M. Zhang, Phys. Rev. D **104**, 095016 (2021).
[57] Q. Yang and S. Dong, Phys. Lett. B **843**, 138004 (2023).
[58] T. W. Kephart and T. J. Weiler, Phys. Rev. Lett. **58**, 171 (1987).
[59] T. W. Kephart and T. J. Weiler, Phys. Rev. D **52**, 3226 (1995).
[60] A. Caputo, M. Regis, M. Taoso, and S. J. Witte, J. Cosmol. Astropart. Phys. 03 (2019) 027.
[61] A. Hook, Phys. Rev. Lett. **120**, 261802 (2018).
[62] L. Di Luzio, B. Gavela, P. Quilez, and A. Ringwald, J. High Energy Phys. 05 (2021) 184.
[63] A. Banerjee, G. Perez, M. Safronova, I. Savoray, and A. Shalit, J. High Energy Phys. 10 (2023) 042.
[64] A. Arza and P. Sikivie, Phys. Rev. Lett. **123**, 131804 (2019).
[65] M. A. Buen-Abad, J. Fan, and C. Sun, Phys. Rev. D **105**, 075006 (2022).
[66] A. Arza and E. Todarello, Phys. Rev. D **105**, 023023 (2022).
[67] See Supplemental Material at http://link.aps.org/supplemental/10.1103/PhysRevD.109.055026 for the derivation of the signal power in method 2.
[68] J. Diemand, M. Kuhlen, P. Madau, M. Zemp, B. Moore, D. Potter, and J. Stadel, Nature (London) **454**, 735 (2008).
[69] P. Sikivie and Q. Yang, Phys. Rev. Lett. **103**, 111301 (2009).

[70] E. W. Kolb and I. I. Tkachev, Phys. Rev. Lett. **71**, 3051 (1993).
[71] D. F. Jackson Kimball, D. Budker, J. Eby, M. Pospelov, S. Pustelny, T. Scholtes, Y. V. Stadnik, A. Weis, and A. Wickenbrock, Phys. Rev. D **97**, 043002 (2018).
[72] M. Pospelov, S. Pustelny, M. P. Ledbetter, D. F. Jackson Kimball, W. Gawlik, and D. Budker, Phys. Rev. Lett. **110**, 021803 (2013).
[73] T. Gherghetta and A. Shkerin, Phys. Rev. D **108**, 095009 (2023).
[74] H.-Y. Schive, T. Chiueh, and T. Broadhurst, Nat. Phys. **10**, 496 (2014).
[75] J. Veltmaat, J. C. Niemeyer, and B. Schwabe, Phys. Rev. D **98**, 043509 (2018).
[76] J. Veltmaat, B. Schwabe, and J. C. Niemeyer, Phys. Rev. D **101**, 083518 (2020).
[77] M. P. van Haarlem *et al.*, Astron. Astrophys. **556**, A2 (2013).
[78] A. Konovalenko *et al.*, Exp. Astron. **42**, 11 (2016).
[79] G. Taylor, J. Dowell, J. Malins, T. Clarke, N. Kassim, S. Giacintucci, B. Hicks, J. Kooi, W. Peters, E. Polisensky, F. Schinzel, and K. Stovall, arXiv:1708.00090.
[80] B. W. Stappers *et al.*, Astron. Astrophys. **530**, A80 (2011).
[81] S. W. Ellingson, T. E. Clarke, A. Cohen, J. Craig, N. E. Kassim, Y. Pihlstrom, L. J. Rickard, and G. B. Taylor, Proc. IEEE **97**, 1421 (2009).
[82] N. Kassim, S. White, P. Rodriquez, J. Hartman, B. Hicks, J. Lazio, K. Stewart, J. Craig, G. Taylor, C. Cormier, V. Romero, and F. Jenet, in *Advanced Maui Optical and Space Surveillance Technologies Conference*, edited by S. Ryan (2010), p. E59.
[83] A. R. Thompson, J. M. Moran, and George W. Swenson, Jr., *Interferometry and Synthesis in Radio Astronomy*, 3rd ed. (2017).
[84] S. Ellingson, IEEE Trans. Antennas Propag. **53**, 2480 (2005).
[85] ESA, Gaia data release scenario.